Ishii *et al.*
Progress in Earth and Planetary Science (2024) 11:10
https://doi.org/10.1186/s40645-024-00615-0

Progress in Earth and Planetary Science

RESEARCH ARTICLE

Open Access

Hydrogen partitioning between stishovite and hydrous phase δ: implications for water cycle and distribution in the lower mantle

Takayuki Ishii[1,2*], Giacomo Criniti[2], Narangoo Purevjav[2], Tomoo Katsura[2,3] and Eiji Ohtani[4]

Abstract

Water is transported into the deep mantle by subducting slabs, playing important roles in mantle dynamics and evolution. An aluminous hydrous mineral, phase δ with a main component of AlOOH, has been considered an important water carrier in the lower mantle. Recent studies reported that SiO_2 stishovite can accommodate weight percent levels of water, indicating another important water carrier in the lower mantle. However, which mineral can mainly carry water is not clear yet. Recent hydrous phase relation studies reported that stishovite is depleted in alumina when coexisting with hydrous phase δ, in which water content of stishovite was not investigated. In this study, we investigated hydrogen partitioning between stishovite and hydrous phase δ at 24–28 GPa and 1000–1200 °C by means of Kawai-type multi-anvil press in combination with Fourier-transform infrared spectroscopy at ambient conditions on recovered samples. Fourier-transform infrared spectra of recovered stishovites showed that water contents of stishovite coexisting with hydrous phase δ were limited to up to ~500 ppm. This indicates that coexisting hydrous phase δ causes not only depletion in alumina but also in hydrogen in stishovite and therefore mainly transports water in a cold subducting slab. Once hydrous phase δ becomes thermally unstable, alumina and water contents in silica minerals are increased by the chemical reaction between SiO_2 and AlOOH, and aluminous silica minerals such as stishovite and $CaCl_2$-type phase will be a main water carrier in the lower mantle. Presence of small-scale seismic scatterers observed around 1900 km depth, which was considered to be caused by a transition from almost pure SiO_2 stishovite to $CaCl_2$-type phase, might also be able to be explained by the phase transition of stishovite coexisting with hydrous phase δ.

Keywords Water cycle, Mantle, Subducting slab, Hydrous mineral, Nominally anhydrous mineral, Multi-anvil press

1 Introduction

The transportation process of water into the deep mantle is important for understanding the structure and dynamics and the chemical evolution of the Earth because the physical and chemical properties such as melting phase relations, rheology, electrical and thermal conductivity of minerals and rocks in water-bearing systems can be significantly different from those of the dry system (e.g., Thompson 1992; Wang et al. 2006; Kohlstedt 2006; Marzotto et al. 2020). The water solubility of nominally anhydrous minerals and stability of hydrous minerals are therefore essential to clarify the water transport process in the mantle. The discovery of water-rich minerals

*Correspondence:
Takayuki Ishii
takayuki.ishii@okayama-u.ac.jp
[1] Institute for Planetary Materials, Okayama University, Misasa, Japan
[2] Bayerisches Geoinstitut, University of Bayreuth, Universitätsstraße 30, 95447 Bayreuth, Germany
[3] Center for High Pressure Science and Technology Advanced Research, Beijing 100094, China
[4] Department of Earth Science, Graduate School of Science, Tohoku University, Sendai 980-8578, Japan

such as hydrous ringwoodite, superhydrous phase B, and hydrous phase egg as diamond inclusions suggest that water is transported at least into the mantle transition zone (Wirth et al. 2007; Pearson et al. 2014; Tschauner et al. 2018). On the other hand, water transport and its distribution in the lower mantle are poorly understood. Oceanic island basalt contains more water than mid-ocean ridge basalt, suggesting water-rich sources in the lower mantle (Hirschmann 2006). However, major minerals in lower-mantle peridotitic assemblages such as bridgmanite and ferropericlase have generally limited water solubilities less than 0.1 wt% (e.g., Bolfan-Casanova et al. 2002; Fu et al. 2019).

High-pressure silica polymorphs of stishovite and $CaCl_2$-type phase are major constituents of basaltic crusts, sediments, and continental crustal rocks in the lower mantle (e.g., Irifune et al. 1994; Hirose et al. 1999; Ishii et al. 2012, 2019a, b, 2022a). Recent phase relation studies in SiO_2–H_2O systems reported that these silica phases can accommodate water at the weight percent levels (Lin et al. 2020; Nisr et al. 2020) although other studies showed limited water contents up to several hundred ppm (Litasov et al. 2007; Purevjav et al. 2024). Other studies examined their water storage capacities in systems containing Al_2O_3, an important component in the silica-rich rocks mentioned above, and found that the water incorporation mechanism is different from that in an Al-free system and their water contents increase with temperature. The increases are due to water being stored as the AlOOH component, and the mixing entropy increasing its solubility with temperature (Litasov et al. 2007; Ishii et al. 2022b). Ishii et al. (2022b) showed that the water content in $CaCl_2$-type phase reaches 1.1 wt% at a temperature of 1900 °C, which is even higher than the average mantle (Katsura 2022). The stability of $CaCl_2$-type phase at pressures up to ~ 120 GPa (Murakami et al. 2003) allows the silica-enriched rocks that make up the upper layers of the subducting slab to transport water into the deep lower mantle.

Although aluminous silicas are important water hosts in the lower mantle, subducting slabs can have lower temperatures than the average mantle (Thompson 1992; Ganguly et al. 2009), which may limit their water solubility. An aluminous hydrous mineral, hydrous phase δ with compositions of (Al, Fe, Si, Mg)OOH, is considered to be another lower-mantle water carrier because it is stable at pressures down to the bottom of the lower mantle (e.g., Sano et al. 2008; Duan et al. 2018; Strozewski et al. 2023). A recent phase relation study of a hydrous basalt system reported that stishovite coexists with hydrous phase δ at 25–26 GPa, the pressures at the top of the lower mantle, and at relatively low temperatures of 1000–1200 °C (Liu et al. 2019). Further studies reported that hydrous phase δ is stable at relatively low temperatures up to 1400 °C and pressures of 24–28 GPa in SiO_2–Al_2O_3–H_2O and $MgSiO_3$–Al_2O_3–H_2O systems (Ishii et al. 2022b, c). Although the presence of hydrous phase δ increases the water storage capacity in the silica-enriched rocks, it could limit the AlOOH component and therefore the water storage capacities in the silica minerals. Thus, the solubilities of the AlOOH component in the silica phases coexisting with hydrous phase δ are needed to evaluate the bulk water storage capacity in the silica-enriched rocks.

In this study, we determined the water solubility in stishovite coexisting with hydrous phase δ in a SiO_2–Al_2O_3–H_2O system under water-undersaturated conditions using a multi-anvil press in combination with electron probe microanalysis and Fourier transform infrared spectroscopy (FTIR) after recovery.

2 Methods/experimental

2.1 Starting materials

To measure water content by FTIR, it is necessary to grow stishovite crystals at least to 50 microns due to the limited spatial resolution of conventional FTIR spectrometers. However, it is very difficult to grow stishovite crystals coexisting with hydrous phase δ because the synthesis temperature is relatively low and the coexisting phase hampers grain growth. For this reason, the water contents of stishovite coexisting with hydrous phase δ were determined using pre-synthesized stishovite single crystals annealed at a target pressure and temperature in stishovite-hydrous phase δ matrix.

Our preliminary experiments showed that the alumina content in stishovite coexisting with hydrous phase δ is 0.68–0.81 wt% at the same conditions as this study (Ishii et al. 2022b). Based on this result, single crystals of aluminous stishovite were synthesized at 22 GPa and 1900 °C for 2 h using a powdered mixture of reagent-grade SiO_2 quartz and $Al(OH)_3$ gibbsite at a molar ratio of 99:1 including ~ 0.85 wt% Al_2O_3. The recovered stishovite single crystals have dimensions up to 200–400 μm and an alumina content of 0.64(3) wt% as determined by electron microprobe analysis (Table 2 and Additional file 1: Table S1). The lower alumina content in stishovite may be due to presence of hydrous Al–Si melt (Litasov et al. 2007). The water content was estimated to be 994(44) ppm as an average value using 10 randomly oriented crystals by unpolarized FTIR based on Paterson's (1982) calibration. Single crystal X-ray diffraction of a recovered crystal gave the lattice parameters of $a = 4.18077(7)$ Å, $c = 2.66658(13)$ Å, and the unit cell volume of $V = 46.6086(27)$ Å^3. Further details on the analytical methods are provided in the section below. As for the matrix to be employed in the annealing experiments,

this was obtained by mixing reagent-grade SiO_2 quartz and α-AlOOH boehmite, which was then converted to hydrous phase δ after high pressure–temperature annealing.

2.2 High pressure–temperature experiments

All high-pressure experiments were performed using Kawai-type multi-anvil presses installed at the Bayerisches Geoinstitut, University of Bayreuth. We conducted a pre-synthesis experiment of aluminous stishovite starting crystals at 22 GPa and 1900 °C for 2 h using a 10-MN press with a split-sphere guide block. The pressure calibration was reported in Keppler and Frost (2005). The cell assembly with 4 mm truncation tungsten carbide (WC) anvils and a 10 mm edge octahedron reported in Kawazoe et al. (2017) was adopted. The powdered starting sample was packed in a welded Pt capsule.

The water partitioning experiments between stishovite and hydrous phase δ were carried out at pressures of 24 and 28 GPa and temperatures of 1000–1200 °C for 24 h. The 10-MN press was also used for experiments at 24 GPa, in which the pressure estimation by Keppler and Frost (2005) was also adopted. Experiments at 28 GPa were conducted using the 15-MN press with an Osugi-type guide block, IRIS-15 (Ishii et al. 2016, 2019b). Generated pressures against press load were determined in Liu et al. (2017). A similar cell assembly design to that reported by Liu et al. (2020) was adopted, except for the sample chamber (see Fig. 1) at both conditions. A 7 mm Cr_2O_3-doped MgO pressure medium was combined with tungsten carbide (WC) anvils with 3 mm truncated edge lengths. A cylindrical $LaCrO_3$ heater was inserted into the center of the octahedron. $LaCrO_3$ plugs were placed at both ends of the heater. Some single crystals of the pre-synthesized aluminous stishovite were placed in a welded gold capsule, in which the single crystals were separated from each other by the SiO_2–AlOOH powdered mixture. The sample capsule was placed at the center of the heater, from which it was electrically insulated using an MgO sleeve and two plugs. Sample temperatures were measured at the surface of the capsule using a D-type thermocouple. Ceramic components of the cell assembly ($LaCrO_3$ and MgO parts and pressure media) were fired at 1000 °C for at least 3 h. The sample was first compressed to a desired press load at room temperature and then heated to the target temperature at a rate of 100 °C/min. The target conditions were kept for 24 h with temperature fluctuations of less than ± 5 °C. After keeping the target pressure–temperature conditions for the desired time, the temperature was rapidly decreased to room temperature by shutting off the electric power supply to the heater, and then the cell assembly was slowly decompressed to ambient pressure for 15 h.

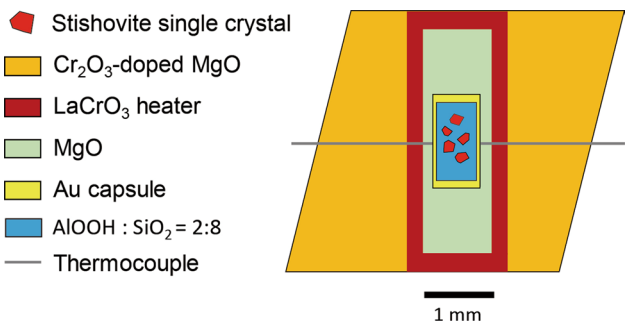

Fig. 1 A schematic drawing of the cell assembly used for the water partitioning experiments

2.3 Analysis of recovered samples

The phases present in the recovered matrix parts were confirmed using a micro-focused X-ray diffractometer with a micro-focus source (IμS) of Co–Kα (Bruker, D8 Discover) in combination with a two-dimensional solid-state detector (VÅNTEC-500).

Single crystals of the starting stishovite were hand-picked from the recovered Pt-capsule and observed under a polarizing microscope. To estimate density of the single crystal stishovite for calculations of their water content based on their FTIR data, an inclusion-free grain with ~ 50 μm in diameter displaying sharp optical extinction was then selected and mounted on glass needles for single-crystal X-ray diffraction measurements. The unit-cell lattice parameters of the single crystal were determined using a Eulerian-geometry Huber single-crystal diffractometer equipped with a Mo*Kα* sealed tube operated at 40 kV and 50 mA and a point detector. The software program *SINGLE* (Angel and Finger 2011) was used to drive the diffractometer and collect diffraction profiles of eight unique reflections, each centered using the 8-position method (King and Finger 1979). The symmetry-constrained lattice parameters were then calculated via a vector least-square refinement.

Recovered crystals were double-side polished to 70–176 μm in thickness for unpolarized FTIR spectroscopy. The FTIR measurements were performed using a Bruker IFS 120 high-resolution spectrometer in combination with a Bruker IR microscope and collected using several randomly oriented crystals. A baseline correction was applied by subtracting from each raw spectrum using a spline function that was fitted outside the OH bands wavenumber region. The water contents in recovered aluminous stishovite were calculated based on the empirical calibration of Paterson (1982):

$$C_{H_2O} = 3 \times \frac{X_i}{150} \int \frac{K(\upsilon)}{(3780-\nu)} d\nu \quad (1)$$

where C_{H2O} is the water content (wt ppm), $K(\nu)$ is the absorption coefficient (cm^{-1}) at a given wave number ν, and X_i is a density factor given as $X_i = 18/2d \times 10^6$, where d is the mineral density (g/l) determined by single-crystal X-ray diffraction and chemical-composition analysis. The absorption coefficients were integrated in the wavenumber range of 2400–3700 cm^{-1}.

The chemical compositions of the crystals were measured using an electron probe microanalyzer with wavelength-dispersive spectrometers (JEOL, JXA-8200) at an accelerating voltage and probe current of 15 kV and 15 nA, respectively. Standard materials were quartz (SiO_2) and synthetic corundum (Al_2O_3) for Si and Al, respectively.

3 Results and discussion

3.1 Water content of pre-synthesized starting aluminous stishovite

Unpolarized FTIR spectra of the pre-synthesized starting stishovite single crystals are shown in Fig. 2. The spectrum of the starting stishovite shows main OH-absorption bands at 2667, 3115, 3240, 3318, and 3403 cm^{-1}. These observations agree with those of stishovites reported by Litasov et al. (2007). Although it is known that stishovite is highly anisotropic (Litasov et al. 2007; Ishii et al. 2022b), we observed limited differences in the unpolarized FTIR profiles of 10 crystals with random crystal orientation, resulting in water contents of 940–1059 ppm. Thus, the average water content of 993 ppm was obtained with one standard deviation of the mean of 44 ppm. The aluminum and hydrogen contents of the starting stishovite were estimated to be 0.75(4) mol% and 0.66(3) mol%, respectively, indicating that the Al/H ratio is close to 1. Previous studies reported Al/H ratios between 2 and 7 (Litasov et al. 2007; Zhang et al. 2022; Ishii et al. 2022b), indicating a high concentration of oxygen vacancy. Thus, the present starting stishovite has a higher Al/H ratio than previously reported. This is probably because our stishovite was synthesized at a higher temperature of 1900 °C than those in previous studies (1200–1800 °C) (Litasov et al. 2007; Ishii et al. 2022b). Ishii et al. (2022b) reported a positive temperature dependence of water content in aluminous silica phases coupled with an increase in the alumina concentration close to or under alumina saturated conditions. On the other hand, since our stishovite with the limited alumina content was synthesized quite far from the alumina saturated conditions, the present experimental condition is not the same as the previous conditions with much more alumina. However, it would be possible to incorporate more hydrogen by a possible positive temperature dependence of the AlOOH content instead of oxygen vacancy formation. This hypothesis is supported by a previous ab initio calculation study (Panero and Stixrude 2004).

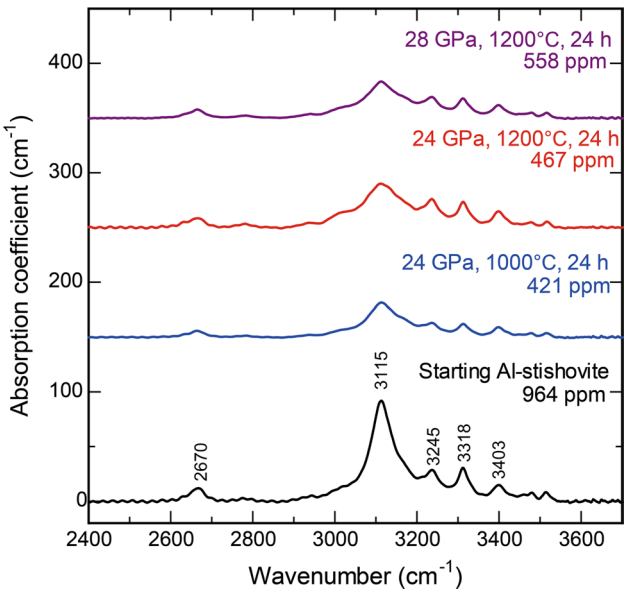

Fig. 2 Representative unpolarized FTIR spectra of recovered stishovite single crystals

3.2 Water contents of aluminous stishovite coexisting with δ-AlOOH

We conducted three water partitioning experiments at 24–28 GPa and 1000–1200 °C (Table 1). Figure 3 shows a representative cross section of a recovered sample capsule including a stishovite single crystal and the matrix part. Powder X-ray diffraction and electron microprobe analysis confirmed that the matrix portion became stishovite with ~0.7 wt% Al_2O_3 and hydrous phase δ with ~4.0 wt% SiO_2 after annealing, showing negligible temperature dependence of the major compositions in the present temperature range. The annealed crystals show the same OH-absorption bands as those of the starting stishovite (Fig. 2). On the other hand, the OH bands of the annealed crystals have lower integrated intensities than those of the starting crystal, indicating a decrease in the water content during annealing. The water contents of aluminous stishovite after annealing have been estimated to be 456–535 ppm corresponding to 0.30–0.35 mol% of hydrogen (Table 2). Thus, the Al/H ratio became ~2, which is close to the trend previously reported (Fig. 4) (Litasov et al. 2007; Zhang et al. 2022; Ishii et al. 2022b). We confirmed that the recovered single crystals were chemically homogeneous based on EPMA and FTIR analyses at different places (Table 2 and Additional

Table 1 Experimental conditions and average water contents of recovered stishovite

Run #	P GPa	T °C	D h	Starting sample	Phase	C_{H2O} ppm	Al_2O_3 content* wt%
H5276	22	1900	3	SiO_2:$Al(OH)_3$ = 99:1	sSt	994(44)	0.64(3)
H5324	24	1000	24	sSt/SiO_2:AlOOH = 8:2	St/St + δ	456(32)	0.63(4)
H5365	24	1200	24	sSt/SiO_2:AlOOH = 8:2	St/St + δ	491(41)	0.64(2)
I1130	28	1200	24	sSt/SiO_2:AlOOH = 8:2	St/St + δ	534(25)	0.62(2)

sSt, Starting stishovite single crystal; St, stishovite; δ, hydrous phase δ

*Average compositions from several grains (see details in Table 2 and Additional file 1: Table S1)

Table 2 Water and alumina contents of recovered stishovites

Run #	Grain #	Water content (ppm)	Al_2O_3 content* (wt%)	H content (mol%)	Thickness (μm)
H5276	1	972	0.59(4)		70
	2	960	0.62(5)		90
	3	1036	0.63(5)		105
	4	940	0.63(5)		80
	5	1059	0.62(6)		70
	6	944	0.63(5)		80
	7	1046	0.65(5)		70
	8	1011	0.65(3)		140
	9	1004	0.66(4)		75
	10	964	0.68(4)		105
	Average	994(44)[§]	0.64(3)	0.66(3)	
H5324	1	426	0.64(3)		140
	2	483	0.64(3)		120
	3	489	0.62(3)		120
	4	463	0.64(4)		100
	5	421	0.60(4)		100
	Average	456(32)[§]	0.63(4)	0.30(2)	
H5365	1	540	0.66(1)		103
	2	475	0.64(2)		150
	3	481	0.66(2)		150
	4	458	0.63(2)		150
	5	545	0.62(3)		120
	6	448	0.64(2)		150
	Average	491(41)[§]	0.64(2)	0.33(2)	
I1130	1	504	0.65(6)		176
	2	511	0.59(4)		176
	3	538	0.63(2)		154
	4	558	0.62(5)		154
	5	558	0.64(5)		154
	Average	534(25)[§]	0.62(2)	0.35(2)	

[§] The errors are expressed as one standard deviation of the mean

*Detailed chemical compositions of recovered stishovite single crystals were shown in Additional file 1: Table S1

file 1: Table S1). The annealing time in this study would be enough to reach equilibrium for hydrogen based on previously determined H diffusivities of minerals such as olivine, its polymorphs, and TiO_2 rutile that has the same structure as stishovite (Ingrin and Blanchard 2006; Chakraborty 2010). We note that alumina contents in stishovite single crystals were consistent within error before/after the partitioning experiments (Table 1, 2 and

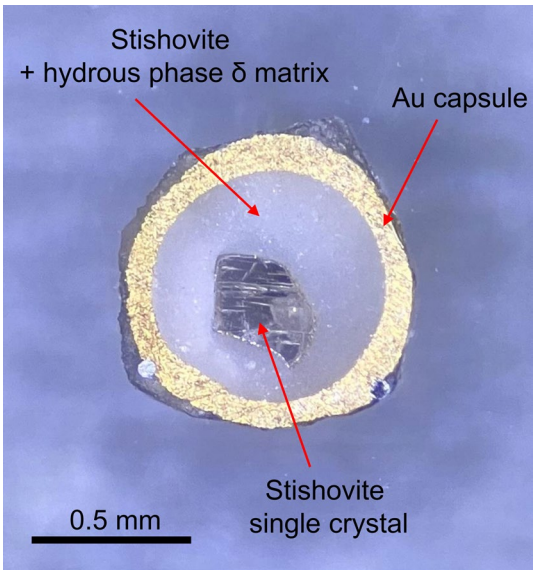

Fig. 3 A representative photo of recovered stishovite after the water partitioning experiment (H5324)

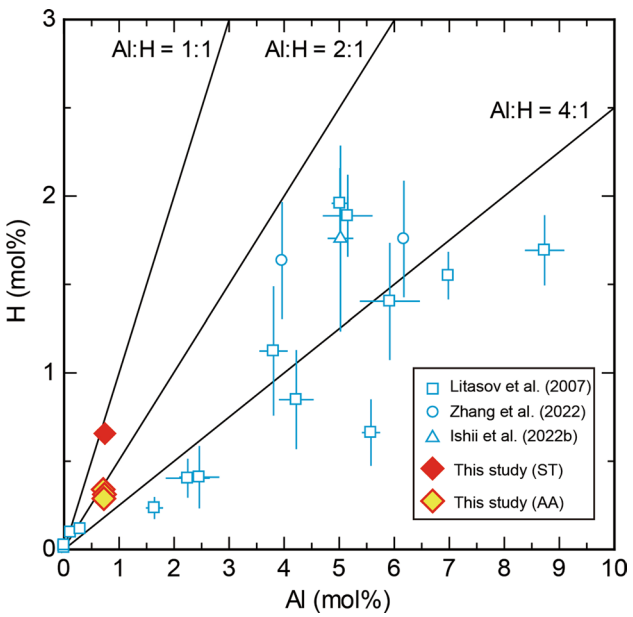

Fig. 4 H^+ contents of stishovite as a function of Al^{3+} content. ST, starting stishovite pre-synthesized; AA, stishovite coexisting with hydrous phase δ after annealing. Some of stishovites in previous studies coexist with liquid phase or hydrous phase egg. Errors of the data from this study are within the size of the symbol

Additional file 1: Table S1). Alumina contents of stishovite in the matrix part (~0.7 wt%) appear to be slightly higher than those of the single crystals (0.59–0.67 wt%). While these values are often in agreement with each other within their mutual uncertainties, it is also possible that Al may have not completely reached chemical equilibrium during the experiments. In the latter case, for an Al/H ratio of 2 (Fig. 4), the water content would increase by only a few tens ppm at the Al content in the matrix part, which is anyway within two standard deviations of the analytical error on the H_2O concentration. Thus, such a small difference in alumina content does not change our conclusions. This result suggests strong water partitioning into hydrous phase δ and is consistent with water partitioning between nominally anhydrous minerals and hydrous minerals in other systems such as bridgmanite and hydrous phase δ/D and olivine polymorphs and hydrous minerals (Ishii and Ohtani 2021, Ishii et al. 2022c).

3.3 Water transport in the lower mantle

Here, we discuss water transport in the mantle. Down to the mantle transition zone, subducted slabs transport water mainly as dense hydrous magnesium silicates such as phase A, superhydrous phase B, and phase D (Litasov and Ohtani 2003; Liu et al. 2019). On the other hand, in the lower mantle, a solid solution between hydrous phase δ and H may crystallize in basaltic and peridotitic layers when the slab temperature is relatively lower than the average mantle (Liu et al. 2019; Nishi et al. 2015; Ishii et al. 2022c). As mentioned earlier, although the nominally anhydrous minerals in the lower mantle, such as bridgmanite and ferropericlase, are almost dry even under water-saturated conditions (e.g., Bolfan-Casanova et al. 2002; Fu et al. 2019), the presence of hydrous phase δ further facilitates dehydration of these minerals and stishovite (Ishii et al. 2022c; this study) and can destabilize alkali element- and alumina-rich minerals, such as the aluminous phases of calcium ferrite phase and hexagonal phase (Ishii et al. 2023), due to the strong alumina and water partitioning to hydrous phase δ.

Recent experimental and theoretical studies suggested that the water solubility of davemaoite is up to a few weight percent, although the unquenchability prevents a definitive conclusion (Chen et al. 2020; Shim et al. 2022). Chen et al. (2020) demonstrated that davemaoite may be hydrous even when coexisting with hydrous phase δ based on the crystal structure change in davemaoite from cubic to tetragonal and the volume reduction relative to the dry sample by a laser-heated diamond anvil cell. The strong alumina and water partitioning to hydrous phase δ against bridgmanite and stishovite suggests that davemaoite is also alumina- and water-depleted at least when coexisting with hydrous phase δ, although further experiments are needed to investigate the water solubility of davemaoite in the $CaSiO_3$-AlOOH system.

Therefore, we suggest that a main water carrier would be hydrous phase δ-H solid solution in a relatively low

temperature slab. Because slab temperature should be gradually increasing, hydrous phases are likely to decompose at some depths when the slab temperature approaches that of the average lower mantle (Katsura 2022). After dehydration, the released water will react with aluminous silica phases, resulting in the water carrier being replaced by hydrous aluminous silicas such as stishovite and $CaCl_2$-type phase due to their positive temperature dependence of alumina and water contents (Ishii et al. 2022b).

3.4 Seismic scatterers in the lower mantle

Seismological studies found ~ 10 km thick seismic scattering bodies with lower shear-wave velocities and higher densities than the surrounding mantle between 700 and 1900 km depths (e.g., Kaneshima 2019 and references therein). These observations have been explained by the second-order ferroelastic transition from stishovite to $CaCl_2$-type phase in subducted basaltic crusts because the transition pressure decreases with increasing alumina and water content (e.g., Lakshtanov et al. 2007; Zhang et al. 2022; Ishii et al. 2022b; Criniti et al. 2023). Thus, the deepest seismic scatterers around 1900 km depth were interpreted by the transition in dry and almost pure SiO_2 system (e.g., Nomura et al. 2010; Fischer et al. 2018), implying that subducted basaltic crusts at this depth could be dry because stishovite in a dry basaltic crust is alumina depleted (Irifune et al. 1994; Ishii et al. 2019a, b, 2022a). The present study suggests that even low-temperature hydrous basaltic crust with hydrous phase δ may be compatible with these observations as alumina and water will be strongly partitioned into hydrous phase δ. We note that stishovite coexisting with hydrous phase δ has a small amount of alumina and water as described above and even such small amounts of alumina and water may affect the transition pressure. Since previous studies demonstrated a reduction in the transition pressure by H and Al incorporation in relatively high alumina- and water-bearing samples with more than 3 wt% and 0.25 wt%, respectively (e.g., Lakshtanov et al. 2007; Zhang et al. 2022; Criniti et al. 2023), further studies are needed to clarify the effect of low H and Al incorporation.

4 Conclusions

We have determined water contents of aluminous stishovite coexisting with hydrous phase δ at 24–28 GPa and 1000–1200 °C using a Kawai-type multi-anvil press in combination with FTIR measurements of recovered stishovites at ambient pressure. Aluminous stishovite coexisting with hydrous phase δ is depleted in alumina (< 1 wt%) and has ~ 500 ppm water, showing a strong water and alumina partitioning to hydrous phase δ. The present results in addition to previous results of water solubility of nominally anhydrous lower-mantle minerals suggest that hydrous phase δ is a main water carrier in the lower mantle when a subducting slab is at relatively low temperatures compared with the average mantle. Once the subducting slab becomes warm enough to trigger the dehydration of hydrous minerals, aluminous silica minerals such as stishovite and $CaCl_2$-type phase will become the main water carriers. Seismic scatterers observed around 1900 km depth may be explained by the transition of Al, H-poor stishovite to $CaCl_2$-type phase coexisting with hydrous phase δ at low temperatures.

Abbreviation

FTIR Fourier transform infrared spectroscopy

Supplementary Information

The online version contains supplementary material available at https://doi.org/10.1186/s40645-024-00615-0.

Additional file 1: Table S1. Chemical compositions for major components of recovered stishovite single crystals.

Acknowledgements

We thank H. Fischer and R. Njul for the preparation of cell assemblies and thin-section samples, respectively. We thank the Editor of Craig R. Bina and two anonymous reviewers for their constructive comments.

Author contributions

TI and EO designed the research topic. TI and NP discussed the preliminary results at the initial stage of this project. TI carried out the high-pressure experiments and measured and analyzed FTIR spectra and micro-focus XRD data of recovered samples. GC measured and analyzed the single crystal XRD data. TI wrote the original draft and revised it by including inputs from GC, NP, TK, and EO. All authors read and approved the final manuscript.

Funding

This work was funded by the European Research Council (ERC) under the European Union's Horizon 2020 research and innovation programme (Proposal No. 787,527) to T.K. and a DFG grant (IS350/1-1) to T.I. The National Natural Science Foundation of China (NSFC) also supported this work (grant no.: 92158206 to R. Tao and T.I.). E.O. and T.I. were supported by the Kakenhi Grant Number JP20H00187 and JP23K19067, respectively. E.O. was also supported by the research award from the Alexander von Humboldt foundation.

Availability of data and materials

FTIR data that support the findings of this study are available on Zenodo (https://doi.org/10.5281/zenodo.8302693).

Declarations

Competing interests

The authors declare that they have no competing interest.

Received: 5 September 2023 Accepted: 21 February 2024
Published online: 27 February 2024

References

Angel RJ, Finger LW (2011) SINGLE: a program to control single-crystal diffractometers. J Appl Cryst 44:247–251

Bolfan-Casanova N, Mackwell S, Keppler H, McCammon C, Rubie DC (2002) Pressure dependence of H solubility in magnesiowüstite up to 25 GPa: implications for the storage of water in the Earth's lower mantle. Geophys Res Lett 29:89–91

Chakraborty S (2010) Diffusion coefficients in olivine, wadsleyite and ringwoodite. Rev Mineral Geochem 72:603–639

Chen H, Leinenweber K, Prakapenka V, Prescher C, Meng Y, Bechtel H, Kunz M, Shim SH (2020) Possible H_2O storage in the crystal structure of $CaSiO_3$ perovskite. Phys Earth Planet Inter 299:106412

Criniti G, Ishii T, Kurnosov A, Glazyrin K, Boffa Ballaran T (2023) High-pressure phase transition and equation of state of hydrous Al-bearing silica. Am Mineral

Duan Y, Sun N, Wang S, Li X, Guo X, Ni H, Prakapenka VB, Mao Z (2018) Phase stability and thermal equation of state of δ-AlOOH: implication for water transportation to the deep lower mantle. Earth Planet Sci Lett 494:92–98

Fischer RA, Campbell AJ, Chidester BA, Reaman DM, Thompson EC, Pigott JS, Prakapenka VB, Smith JS (2018) Equations of state and phase boundary for stishovite and $CaCl_2$-type SiO_2. Am Mineral 103:792–802

Fu S, Yang J, Karato S, Vasiliev A, Presniakov MY, Gavriliuk AG (2019) Water concentration in single-crystal (Al, Fe)-bearing bridgmanite grown from the hydrous melt: Implications for dehydration melting at the topmost lower mantle. Geophys Res Lett 46:10346–10357

Ganguly J, Freed AM, Saxena SK (2009) Density profiles of oceanic slabs and surrounding mantle: integrated thermodynamic and thermal modeling, and implications for the fate of slabs at the 660 km discontinuity. Phys Earth Planet Inter 172:257–267

Hirose K, Fei Y, Ma Y, Mao HK (1999) The fate of subducted basaltic crust in the Earth's lower mantle. Nature 397:53

Hirschmann MM (2006) Water, melting, and the deep Earth H_2O cycle. Annu Rev Earth Planet Sci 34:629–653

Ingrin J, Blanchard M (2006) Diffusion of hydrogen in minerals. Rev Mineral Geochem 62:291–320

Irifune T, Ringwood AE, Hibberson WO (1994) Subduction of continental crust and terrigenous and pelagic sediments: an experimental study. Earth Planet Sci Lett 126:351–368

Ishii T, Ohtani E (2021) Dry metastable olivine and slab deformation in a wet subducting slab. Nat Geosci 14:526–530

Ishii T, Kojitani H, Akaogi M (2012) High-pressure phase transitions and subduction behavior of continental crust at pressure–temperature conditions up to the upper part of the lower mantle. Earth Planet Sci Lett 357:31–41

Ishii T, Shi L, Huang R, Tsujino N, Druzhbin D, Myhill R, Li Y, Wang L, Yamamoto T, Miyajima N, Kawazoe T, Nishiyama N, Higo Y, Tange Y, Katsura T (2016) Generation of pressures over 40 GPa using Kawai-type multi-anvil press with tungsten carbide anvils. Rev Sci Instrum 87:024501

Ishii T, Kojitani H, Akaogi M (2019a) Phase relations of harzburgite and MORB up to the uppermost lower mantle conditions: precise comparison with pyrolite by multisample cell high-pressure experiments with implication to dynamics of subducted slabs. J Geophys Res Solid Earth 124:3491–3507

Ishii T, Liu Z, Katsura T (2019b) A breakthrough in pressure generation by a Kawai-type multi-anvil apparatus with tungsten carbide anvils. Engineering 5:434–440

Ishii T, Miyajima N, Criniti G, Hu Q, Glazyrin K, Katsura T (2022a) High pressure-temperature phase relations of basaltic crust up to mid-mantle conditions. Earth Planet Sci Lett 584:117472

Ishii T, Criniti G, Ohtani E, Purevjav N, Fei H, Katsura T, Mao HK (2022b) Superhydrous aluminous silica phases as major water hosts in high-temperature lower mantle. Proc Natl Acad Sci 119:e2211243119

Ishii T, Ohtani E, Shatskiy A (2022c) Aluminum and hydrogen partitioning between bridgmanite and high-pressure hydrous phases: Implications for water storage in the lower mantle. Earth Planet Sci Lett 583:117441

Ishii T, Criniti G, Wang X, Glazyrin K, Ballaran TB (2023) Synthesis and structural analysis of $CaFe_2O_4$-type single crystals in the $NaAlSiO_4$-$MgAl_2O_4$-Fe_3O_4 system. Am Mineral 108:217–221

Kaneshima S (2019) Seismic scatterers in the lower mantle near subduction zones. Geophys J Int 219:S2–S20

Katsura T (2022) A revised adiabatic temperature profile for the mantle. J Geophys Res Solid Earth 127:e2021JB023562

Kawazoe T, Ohira I, Ishii T, Boffa Ballaran T, McCammon C, Suzuki A, Ohtani E (2017) Single crystal synthesis of δ-(Al, Fe)OOH. Am Mineral 102:1953–1956

Keppler H, Frost DJ (2005) Introduction to minerals under extreme conditions. In: Miletich R (ed) Mineral behavior at extreme conditions. Eötvös University Press, Budapest

King HE, Finger LW (1979) Diffracted beam crystal centering and its application to high-pressure crystallography. J Appl Cryst 12:374–378

Kohlstedt DL (2006) The role of water in high-temperature rock deformation. Rev Mineral Geochem 62:377–396

Lakshtanov DL, Sinogeikin SV, Litasov KD, Prakapenka VB, Hellwig H, Wang J, Sanches-Valle C, Perrillat JP, Chen B, Somayazulu M, Li J, Ohtani E, Bass DJ (2007) The post-stishovite phase transition in hydrous alumina-bearing SiO_2 in the lower mantle of the earth. Proc Natl Acad Sci 104:13588–13590

Lin Y, Hu Q, Meng Y, Walter M, Mao HK (2020) Evidence for the stability of ultrahydrous stishovite in Earth's lower mantle. Proc Natl Acad Sci 117:184–189

Litasov K, Ohtani E (2003) Stability of various hydrous phases in CMAS pyrolite-H_2O system up to 25 GPa. Phys Chem Miner 30:147–156

Litasov KD, Kagi H, Shatskiy A, Ohtani E, Lakshtanov DL, Bass JD, Ito E (2007) High hydrogen solubility in Al-rich stishovite and water transport in the lower mantle. Earth Planet Sci Lett 262:620–634

Liu Z, Nishi M, Ishii T, Fei H, Miyajima N, Ballaran TB, Ohfuji H, Sakai T, Wang L, Shcheka S, Arimoto T, Tange Y, Higo Y, Irifune T, Katsura T (2017) Phase relations in the system $MgSiO_3$-Al_2O_3 up to 2300 K at lower mantle pressures. J Geophys Res Solid Earth 122:7775–7788

Liu X, Matsukage KN, Nishihara Y, Suzuki T, Takahashi E (2019) Stability of the hydrous phases of Al-rich phase D and Al-rich phase H in deep subducted oceanic crust. Am Mineral 104:64–72

Liu Z, McCammon C, Wang B, Dubrovinsky L, Ishii T, Bondar D, Nakajima A, Tange Y, Higo Y, Cui T (2020) Stability and solubility of the $FeAlO_3$ component in bridgmanite at uppermost lower mantle conditions. J Geophys Res Solid Earth 125:e2019JB018447

Marzotto E, Hsieh WP, Ishii T, Chao KH, Golabek GJ, Thielmann M, Ohtani E (2020) Effect of water on lattice thermal conductivity of ringwoodite and its implications for the thermal evolution of descending slabs. Geophys Res Lett 47:e2020GL087607

Murakami M, Hirose K, Ono S, Ohishi Y (2003) Stability of $CaCl_2$-type and α-PbO_2-type SiO_2 at high pressure and temperature determined by in-situ X-ray measurements. Geophys Res Lett 30:11

Nishi M, Irifune T, Gréaux S, Tange Y, Higo Y (2015) Phase transitions of serpentine in the lower mantle. Phys Earth Planet Inter 245:52–58

Nisr C, Chen H, Leinenweber K, Chizmeshya A, Prakapenka VB, Prescher C, Tkachev SN, Meng Y, Liu Z, Shim SH (2020) Large H_2O solubility in dense silica and its implications for the interiors of water-rich planets. Proc Natl Acad Sci 117:9747–9754

Nomura R, Hirose K, Sata N, Ohishi Y (2010) Precise determination of post-stishovite phase transition boundary and implications for seismic heterogeneities in the mid-lower mantle. Phys Earth Planet Inter 183:104–109

Panero WR, Stixrude LP (2004) Hydrogen incorporation in stishovite at high pressure and symmetric hydrogen bonding in δ-AlOOH. Earth Planet Sci Lett 221:421–431

Paterson M (1982) The determination of hydroxyl by infrared absorption in quartz, silicate glasses and similar materials. Bull Mineral 105:20–29

Pearson D, Brenker F, Nestola F, McNeill J, Nasdala L, Hutchison M, Matveev S, Mather K, Silversmit G, Schmitz S (2014) Hydrous mantle transition zone indicated by ringwoodite included within diamond. Nature 507:221–224

Purevjav N, Fei H, Ishii T, Criniti G, Lin Y, Mao HK, Katsura T (2024) Temperature dependence of H_2O solubility in Al-free stishovite. Geophys Res Lett 51:e2023GL104029

Sano A, Ohtani E, Kondo T, Hirao N, Sakai T, Sata N, Ohishi Y, Kikegawa T (2008) Aluminous hydrous mineral δ-AlOOH as a carrier of hydrogen into the core-mantle boundary. Geophys Res Lett 35:L03303

Shim SH, Chizmeshya A, Leinenweber K (2022) Water in the crystal structure of $CaSiO_3$ perovskite. Am Mineral 107:631–641

Strozewski B, Buchen J, Sturhahn W, Ishii T, Ohira I, Chariton S, Lavina B, Zhao J, Toellner TS, Jackson JM (2023) Equation of state and spin crossover of (Al, Fe)-phase H. J Geophys Res Solid Earth 128:e2022JB026291

Thompson AB (1992) Water in the Earth's upper mantle. Nature 358:295–302

Tschauner O, Huang S, Greenberg E, Prakapenka V, Ma C, Rossman GR, Shen AH, Zhang D, Newville M, Lanzirotti A, Tait K (2018) Ice-VII inclusions in diamonds: evidence for aqueous fluid in Earth's deep mantle. Science 359:1136–1139

Wang D, Mookherjee M, Xu Y, Karato SI (2006) The effect of water on the electrical conductivity of olivine. Nature 443:977–980

Wirth R, Vollmer C, Brenker F, Matsyuk S, Kaminsky F (2007) Inclusions of nanocrystalline hydrous aluminium silicate "Phase Egg" in superdeep diamonds from Juina (Mato Grosso State, Brazil). Earth Planet Sci Lett 259:384–399

Zhang Y, Fu S, Karato SI, Okuchi T, Chariton S, Prakapenka VB, Lin JF (2022) Elasticity of hydrated Al-bearing stishovite and post-stishovite: Implications for understanding regional seismic VS anomalies along subducting slabs in the lower mantle. J Geophys Res Solid Earth 127:e2021JB023170

Publisher's Note